Wave-optics description of amplified spontaneous emission

J. C. Garrison, B. Ritchie, H. Nathel, C. K. Hong, and L. Minner
Lawrence Livermore National Laboratory, University of California, Livermore, California 94550
(Received 25 October 1990)

Paraxial Maxwell-Bloch theory is used to describe amplified spontaneous emission (ASE) in strongly inverted media. Counterpropagation of waves coupled through gain saturation and diffraction, and pumping by a laser beam which propagates transverse to the amplifier are included in the treatment. The reactive part of the medium polarization is calculated by population-rate equations in the limit of rapid dephasing of the atomic dipoles. The spontaneous emission noise source needed for the numerical simulation of Maxwell's equations is derived from microscopic theory by coarse-graining, thereby establishing the compatibility of the spherically symmetric microscopic source with paraxial propagation theory. The three coupled Maxwell equations for the counterpropagating ASE waves and the transversely propagating pump wave are solved numerically in time and two spatial dimensions. This simulation is used to calculate the longitudinal profile of the transverse fluorescence, which measures the saturation of the gain, the longitudinal profile of the transmitted pump wave, which measures the saturation of pump absorption, and the transverse coherence function of the radiation emitted from the ends of the amplifier.

I. INTRODUCTION

The wave-optics description of amplified spontaneous emission (ASE) presents several major difficulties. In the case of strong inversion, i.e., when the lower level of the ASE transition depopulates very rapidly, transverse pumping produces two ASE waves which propagate toward the forward and backward ends of a pencil-shaped amplifier and are coupled through the atomic response.[1] The nonlinear coupling results in gain saturation, and the steady-state intensity at either end of the amplifier is approximately limited by $G_0L/2$ (in units of the saturation intensity), where G_0 is the small-signal gain and L is the amplifier length. The atomic response is described by population-rate equations, which are the result of the adiabatic elimination of the off-diagonal or coherence matrix elements from the atomic density matrix. This is appropriate when the decay of the atomic dipole moment is much faster than the rate of growth of ASE radiation, i.e., when $T_2 \ll (G_0c)^{-1}$. In the more familiar case of swept gain pumping the propagation is unidirectional; therefore, the coupling of counterpropagating waves through gain saturation does not occur,[2,3] and the calculation of unidirectional propagation, including transverse effects, e.g., diffraction, is readily carried out in the retarded-time frame, in which the time (t) and propagation direction (z) are combined into $t-z/c$. Thus a major difficulty in a two-way calculation is the need to treat t and z as separate, independent variables if complete generality is to be attained.

Another major difficulty and source of confusion in a wave-optics description of ASE is the prescription for augmenting Maxwell's equation with a phenomenological source. The source should simulate spontaneous emission noise in the appropriate $T_2 \ll (G_0c)^{-1}$ limit and be correctly normalized with respect to the single-atom spontaneous emission rate (i.e., the Einstein A coefficient). Microscopic noise theory is used to find a source which satisfies these criteria, and is appropriate for paraxial wave propagation with diffraction along the two directions transverse to the propagation axis. This analysis shows that the correct treatment of diffraction automatically leads to the appearance of a solid-angle factor in the source strength. This replaces the intuitive argument, often used in plane-wave calculations, that the source strength should be reduced by a solid-angle factor in order to represent the dominance of the strongly amplified near axial waves.[4,5]

The elementary aspects of ASE have been understood for a long time, but new experiments, especially those oriented towards applications, have created renewed interest in a more microscopic and detailed approach to this problem. The older model calculations were usually restricted to ray tracing or at most plane-wave optics, and could not address issues, such as transverse coherence, which are important for certain applications. Recent experiments involving laser-pumped dye solutions,[6] and the continuing work on plasmas in which some ionic species are selectively excited, as in a line pumped x-ray laser scheme,[7] are examples of strongly inverted media which require a more detailed treatment. These systems are approximately described by the model presented below, as well as by recent closely related work.[8]

In Sec. II we describe the propagation theory used in our simulations. We present the stochastic scheme used to simulate the quantum equations in Sec. III, and in Sec. IV we give some characteristic results and some comparisons to experiment. A summary is given in Sec. V.

II. THEORY OF PROPAGATION IN STRONGLY INVERTED MEDIA

In this section we make use of a quantum propagation theory (hereafter called QASE) formulated in Ref. 1 to

describe bidirectional propagation of ASE signals. We also allow for transverse propagation of a pump laser beam. The active medium occupies a rectangular region with dimensions d (x axis), h (y axis), and L (z axis), where $L \gg d,h$. For applications involving laser pumping, we assume that the sample is pumped through the input ($x=-d/2$) face by a long pulse (e.g., a pulse duration of 100 transit times) laser beam which is uniform in y and z and propagates in the positive x direction. With this geometry two ASE signals will grow up from quantum noise and counterpropagate along the z axis. Our propagation simulations include the effects of diffraction and transverse gain profile in the x direction, cross-saturation between the ASE signals and the pump, and nonlinear coupling between the two ASE beams.

A. Quantum paraxial approximation

For the geometry used in our model, the electromagnetic fields can be treated in a paraxial (slowly varying envelope) approximation. The total (quantized) ASE field is given by the ansatz

$$\mathbf{E}(\mathbf{x},t)=\sum_{\sigma}[\mathcal{E}_{\sigma}(\mathbf{x},t)\boldsymbol{\eta}e^{i(\sigma kz-\omega t)}+\text{H.c.}]\ , \tag{2.1}$$

where $\sigma\in\{+,-\}$ labels the counterpropagating waves, and the operators $\mathcal{E}_{\sigma}$ are slowly varying on the scale of the carrier wavelength and frequency. In (2.1) we have made the simplifying assumption that only one polarization state is excited in the ASE field. The field operators satisfy the commutation relations

$$[\mathcal{E}_{\sigma}(\mathbf{x},t),\mathcal{E}_{\rho}(\mathbf{x}',t)]=\frac{2\pi\hbar\omega}{\epsilon}\delta_{\sigma\rho}\delta(\mathbf{x}-\mathbf{x}') \tag{2.2}$$

and the paraxial equation

$$\left[\sigma\frac{\partial}{\partial z}+\frac{1}{c_0}\frac{\partial}{\partial t}-\frac{i}{2k}\nabla^2\right]\mathcal{E}_{\sigma}=\frac{2\pi ik}{\epsilon}\mathcal{P}_{\sigma}\ , \tag{2.3}$$

where $\mathcal{P}_{\sigma}$ is the macroscopic polarization operator that couples to $\mathcal{E}_{\sigma}$, ϵ is the (linear) dielectric constant of the medium, $c_0=c/\sqrt{\epsilon}$ is the speed of light in the medium, and $k=\omega/c_0$.

In experiments with dye solutions, it is convenient to pump the sample with a suitable laser. The pump laser is described by a classical field

$$\mathbf{E}_P(\mathbf{x},t)=\mathcal{E}_P(\mathbf{x},t)\boldsymbol{\eta}_P e^{i(k_P z-\omega)}+\text{c.c.}\ , \tag{2.4}$$

with polarization vector $\boldsymbol{\eta}_P$. The slowly varying complex amplitude $\mathcal{E}_P$ satisfies

$$\left[\frac{\partial}{\partial x}+\frac{1}{c_0}\frac{\partial}{\partial t}-\frac{i}{2k_P}\nabla^2\right]\mathcal{E}_P=\frac{2\pi ik_P}{\epsilon}\langle\mathcal{P}_P\rangle\ , \tag{2.5}$$

where $k_P=\omega_P/c_0$, and $\langle\mathcal{P}_P\rangle$ is the ensemble average of the component of the macroscopic polarization operator which couples to the pump wave.

B. Four-level atom model

A detailed description of the dynamics of the various gain media would be both extremely difficult and not very useful. In order to obtain a manageable model, we follow the usual procedure in which the levels involved in pumping and stimulated emission are treated as an effective four-level atom[9] with the level scheme shown in Fig. 1. The complex level structures of the actual medium are represented by discrete levels with phenomenological decay rates, γ_{α} ($\alpha\in\{h,a,b,g\}$). In our model $\gamma_g=0$, and γ_a is the spontaneous radiative decay rate of the upper lasing level. The rates γ_b and γ_h correspond to very rapid decays which are radiative for x-ray lasers and nonradiative for dyes. In all cases $\gamma_a \ll \gamma_b$ and $\gamma_b \approx \gamma_h$.

In QASE we describe the atoms by the operators $R_{\alpha\beta}$:

$$R_{\alpha\alpha}=|\alpha\rangle\langle\alpha|,\quad R_{ba}=|b\rangle\langle a|e^{i\omega t}\ , \tag{2.6}$$

where $\alpha,\beta\in\{h,a,b,g\}$, $R_{\alpha\beta}=R^{\dagger}_{\beta\alpha}$, $\omega=(\epsilon_a-\epsilon_b)/\hbar$, and ϵ_{α} is the energy of the αth level. The dipole operator for the ASE transition is $M_{ba}=\mu_{ba}R_{ba}$, where $\mu_{ba}=\boldsymbol{\eta}\cdot\boldsymbol{\mu}_{ba}$ is the projection of the vector matrix element along the direction $\boldsymbol{\eta}$ of the signal polarization. Standard operator noise theory[1,10] yields the dynamical equations for the atomic operators:

$$\frac{\partial}{\partial t}R_{ba}=-\gamma_{ab}R_{ba}-\frac{i}{3\hbar}\sum_{\sigma}e^{i\sigma kz}(R_{aa}-R_{bb})\mu_{ab}\mathcal{E}_{\sigma}(x_m)+\Gamma_{ba}\ , \tag{2.7}$$

$$\frac{\partial}{\partial t}R_{aa}=\gamma_h R_{hh}-\gamma_a R_{aa}-\frac{i}{\hbar}\sum_{\sigma}(\mu_{ba}\mathcal{E}^{*}_{\sigma}R_{ba}e^{-i\sigma kz}-\text{H.c.})+\Gamma_{aa}\ , \tag{2.8}$$

$$\frac{\partial}{\partial t}R_{bb}=\gamma_a R_{aa}-\gamma_b R_{bb}+\frac{i}{\hbar}\sum_{\sigma}(\mu_{ba}\mathcal{E}^{*}_{\sigma}R_{ba}e^{-i\sigma kz}-\text{H.c.})+\Gamma_{bb}\ , \tag{2.9}$$

$$\frac{\partial}{\partial t}R_{hh}=-\gamma_h R_{hh}+w_P R_{gg}+\Gamma_{hh}\ , \tag{2.10}$$

$$\frac{\partial}{\partial t}R_{gg}=\gamma_b R_{bb}-w_P R_{gg}+\Gamma_{gg}\ , \tag{2.11}$$

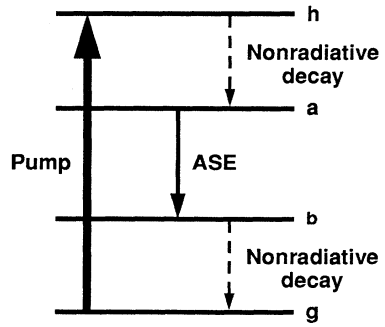

FIG. 1. Four-level-atom model for a rhodamine 6G dye solution. Levels h (width γ_h) and b (width γ_b) represent quasicontinuous vibration bands.

where γ_{ab} $(=1/T_2)$, the dephasing rate for the dipole moment, is given by

$$\gamma_{ab}=\tfrac{1}{2}(\gamma_a+\gamma_b) , \tag{2.12}$$

and w_P is the pumping rate. For laser pumping

$$w_P=P\sigma_P/\hbar\omega_P , \tag{2.13}$$

$$P=\epsilon c_0|\mathcal{E}_P|^2/2\pi , \tag{2.14}$$

where P is the pump intensity, and σ_P is the absorption cross section at the pump wavelength. We impose the adiabaticity condition on the pumping rate as well as the spontaneous decay rate γ_a:

$$\gamma_a \ll \gamma_b, \quad w_P \ll \gamma_b . \tag{2.15}$$

The correlation strengths of the noise operators $\Gamma_{\alpha\alpha}$ and Γ_{ba} are related to the dissipative constants by the fluctuation dissipation theorem.[10] We show in Appendix A that the adiabaticity condition (2.15) guarantees that the population noise terms $\Gamma_{\alpha\alpha}$ are weak compared to the dipole noise Γ_{ba}. We will therefore simplify the general theory of QASE by dropping the $\Gamma_{\alpha\alpha}$'s from (2.7)–(2.11). The dipole noise term satisfies

$$\begin{aligned}\langle \Gamma_{ba}^{\dagger}(t)\Gamma_{ba}(t')\rangle &=(\gamma_b\rho_{aa}+w_P\rho_{gg})\delta(t-t') \\ &\approx \gamma_b\rho_{aa}\delta(t-t') ,\end{aligned} \tag{2.16}$$

where $\rho_{\alpha\alpha}=\langle R_{\alpha\alpha}\rangle$ and $\langle\ \rangle$ indicates an ensemble average.

We next obtain the adiabatic solution of the atomic equations based on the adiabaticity condition (2.15). First consider the population operators R_{bb} and R_{hh}; the adiabatic solution of (2.10) is obtained by neglecting $\partial R_{hh}/\partial t$ to get

$$R_{hh}=\frac{w_P}{\gamma_h}R_{gg} , \tag{2.17}$$

and in the same way adding (2.8) and (2.9) implies

$$R_{bb}=\frac{\gamma_h}{\gamma_b}R_{hh}-\frac{1}{\gamma_b}\frac{\partial}{\partial t}R_{aa} . \tag{2.18}$$

These solutions show that

$$R_{bb}\approx R_{hh}\ll R_{gg} , \tag{2.19}$$

and combining them with (2.11) yields

$$\frac{\partial}{\partial t}R_{aa}+\frac{\partial}{\partial t}R_{gg}\approx 0 . \tag{2.20}$$

Therefore, in the adiabatic limit, the conservation of population becomes

$$R_{aa}+R_{gg}\approx 1 . \tag{2.21}$$

The adiabatic solution of the operator equation (2.7) requires more care because of the rapidly fluctuating noise term. We begin with a formal solution:

$$\begin{aligned}R_{ba}(t)=&R_{ba}(0)e^{-\gamma_{ab}t} \\ &+\int_0^t dt' e^{-\gamma_{ab}(t-t')}S_{\rm coh}(t') \\ &+\int_0^t dt' e^{-\gamma_{ab}(t-t')}\Gamma_{ba}(t')\end{aligned} \tag{2.22}$$

where

$$S_{\rm coh}(t)=-\frac{i\mu_{ab}}{3\hbar}\sum_{\sigma}e^{i\sigma kz}[R_{aa}(t)-R_{bb}(t)]\mathcal{E}_{\sigma}(\mathbf{x},t) , \tag{2.23}$$

and $\mathbf{x}$ is the location of the atom. We put (2.22) into a more convenient form by adding and subtracting the term

$$\int_{-\infty}^0 dt' e^{-\gamma_{ab}(t-t')}\Gamma_{ba}(t') \tag{2.24}$$

to get

$$\begin{aligned}R_{ba}(t)=&\left[R_{ba}(0)-\int_{-\infty}^0 dt' e^{\gamma_{ab}t'}\Gamma_{ba}(t')\right]e^{-\gamma_{ab}t} \\ &+\int_0^t dt' e^{-\gamma_{ab}(t-t')}S_{\rm coh}(t') \\ &+\int_{-\infty}^t dt' e^{-\gamma_{ab}(t-t')}\Gamma_{ba}(t') .\end{aligned} \tag{2.25}$$

In the limit of large γ_{ab}, the first term can be neglected after the transcience interval $1/\gamma_{ab}$, and the integral in the second term can be evaluated by setting the slowly varying term $S_{\rm coh}(t')\approx S_{\rm coh}(t)$; this yields

$$R_{ba}(t)=\frac{S_{\rm coh}(t)}{\gamma_{ab}}+\tilde{\Gamma}_{ba}(t) , \tag{2.26}$$

$$\tilde{\Gamma}_{ba}(t)\equiv\int_{-\infty}^t dt' e^{-\gamma_{ab}(t-t')}\Gamma_{ba}(t') . \tag{2.27}$$

The operator $\tilde{\Gamma}_{ba}(t)$ represents colored noise obtained by filtering the white-noise source $\Gamma_{ba}(t)$. We get the equation for R_{aa} by substituting the adiabatic solutions (2.26) for R_{ba} and (2.17) for R_{hh} into (2.8). In doing so we will introduce a further approximation by neglecting the noise contribution to R_{ba}. This is consistent with our neglect of Γ_{aa}, and it also avoids the complications introduced by a multiplicative noise term.[11] The resulting equation for R_{aa} is then

$$\begin{aligned}\frac{\partial}{\partial t}R_{aa}=&w_P R_{gg}-\gamma_a R_{aa} \\ &-\frac{2|\mu_{ab}|^2}{3\hbar^2\gamma_{ab}}\sum_{\sigma}\sum_{\rho}e^{i(\rho-\sigma)kz}\mathcal{E}_{\sigma}^{\dagger}\mathcal{E}_{\rho} .\end{aligned} \tag{2.28}$$

The constants multiplying the double sum can be recombined in terms of the stimulated emission cross section $\sigma_{\rm ASE}$, and (2.28) can be rewritten as

$$\begin{aligned}\frac{\partial}{\partial t}R_{aa}=&w_P-\left[w_P+\gamma_a+\frac{\gamma_a}{E_0^2}\sum_{\sigma}\mathcal{E}_{\sigma}^{\dagger}\mathcal{E}_{\sigma}\right. \\ &\left.+\frac{\gamma_a}{E_0^2}\sum_{\sigma}e^{2i\sigma kz}\mathcal{E}_{-\sigma}^{\dagger}\mathcal{E}_{\sigma}\right]R_{aa} ,\end{aligned} \tag{2.29}$$

where E_0 and the corresponding intensity I_0 are given by

$$E_0^2=\frac{2\pi}{\epsilon c_0}\frac{\gamma_a\hbar\omega}{\sigma_{\rm ASE}}=\frac{2\pi}{\epsilon c_0}I_0 \ . \tag{2.30}$$

Thus I_0 is the intensity at which the stimulated emission rate equals the spontaneous emission rate. The final term in (2.29) corresponds to direct coupling of the counterpropagating waves through degenerate four-wave mixing. For our present purposes we will neglect this effect; thus (2.29) becomes

$$\frac{\partial}{\partial t}R_{aa}=w_P-\left[w_P+\gamma_a+\frac{\gamma_a}{I_0}\sum_\sigma \mathcal{I}_\sigma\right]R_{aa} \ , \tag{2.31}$$

where $\mathcal{I}_\sigma$, the intensity of the wave $\mathcal{E}_\sigma$, is

$$\mathcal{I}_\sigma=\frac{\epsilon c_0}{2\pi}\mathcal{E}_\sigma^\dagger\mathcal{E}_\sigma \ . \tag{2.32}$$

Finally, we investigate the statistical properties of $\tilde\Gamma_{ba}(t)$ by combining (2.16) and (2.27) to get

$$\langle\tilde\Gamma_{ba}^\dagger(t)\tilde\Gamma_{ba}(t')\rangle=\gamma_b e^{-\gamma_{ab}(t+t')}\times\int_{-\infty}^{t_<}dt_1\rho_{aa}(t_1)e^{2\gamma_{ab}t_1} \ , \tag{2.33}$$

where $t_<\equiv\min(t,t')$. The t_1 integral is dominated by the upper limit, and the average population $\rho_{aa}(t_1)$ is slowly varying so

$$\langle\tilde\Gamma_{ba}^\dagger(t)\tilde\Gamma_{ba}(t')\rangle=\gamma_b\left[\rho_{aa}(t_<)\frac{e^{-\gamma_{ab}|t-t'|}}{2\gamma_{ab}}+O(1/\gamma_{ab}^2)\right]\approx\rho_{aa}(t_<)e^{-\gamma_{ab}|t-t'|} \ , \tag{2.34}$$

where the final form comes from the near identity $2\gamma_{ab}\approx\gamma_b$. This shows that the filtered noise has a nonvanishing correlation time $1/\gamma_{ab}$ and that the correlation function has the finite equal time value

$$\langle\tilde\Gamma_{ba}^\dagger(t)\tilde\Gamma_{ba}(t)\rangle\approx\rho_{aa}(t) \ . \tag{2.35}$$

C. Macroscopic Maxwell-Bloch equations

In this section we will combine the results of Secs. II A and II B to obtain the Maxwell-Bloch operator equations on which our simulations are based. The slowly varying envelope fields $\mathcal{E}_\sigma$ in the ansatz (2.1) are obtained from the microscopic fields by a spatial and temporal coarse-graining procedure. For this purpose we define a volume δV and a time T satisfying (a) $\lambda\ll(\delta V)^{1/3}\ll 1/G_0$, (b) $\delta N=n\delta V\gg 1$, (c) $2\pi/\omega\ll T\ll 1/\gamma_{ab}$, where n is the density of atoms and $G_0=n\sigma_{\rm ASE}$ is the weak signal gain for full inversion. The envelope field $\mathcal{E}_\sigma$ is then given by

$$\mathcal{E}_\sigma(\mathbf{x},t)=\frac{1}{\delta V}\int_{\delta V(\mathbf{x})}d^3x'\frac{1}{T}\int_{t-T/2}^{t+T/2}dt'e^{-i(k\sigma z'-\omega t')}\boldsymbol{\eta}\cdot\mathbf{E}(\mathbf{x}',t') \ , \tag{2.36}$$

where $\delta V(\mathbf{x})$ is a region with volume δV centered on $\mathbf{x}$. We must apply the same averaging procedure to the microscopic polarization density, which is given by

$$p(\mathbf{x},t)=\sum_m\mu_{ba}|b;m\rangle\langle a;m|\delta(\mathbf{x}-\mathbf{x}_m)=\sum_m\mu_{ba}R_{ba}(\mathbf{x}_m,t)e^{-i\omega t}\delta(\mathbf{x}-\mathbf{x}_m) \ , \tag{2.37}$$

where the sum runs over all atoms, and the second line comes from the definition (2.6) of R_{ba}. By averaging $p(\mathbf{x},t)$ we find the source term in the macroscopic paraxial equation (2.3):

$$\mathcal{P}_\sigma(\mathbf{x},t)=\frac{1}{\delta V}\int_{\delta V(\mathbf{x})}d^3x'\frac{1}{T}\int_{t-T/2}^{t+T/2}dt'p_\sigma(\mathbf{x}',t')=\frac{1}{\delta V}\sum_{m\in\delta V(\mathbf{x})}\mu_{ba}R_{ba}(\mathbf{x}_m,t)e^{-i\sigma kz_m} \ , \tag{2.38}$$

where the final sum runs over the atoms contained in $\delta V(\mathbf{x})$, and we have used the fact that $R_{ba}(\mathbf{x}_m,t)$ is slowly varying. We evaluate (2.38) by using the adiabatic solution (2.26) for R_{ba}. This yields two terms, corresponding to $S_{\rm coh}$ and $\tilde\Gamma_{ba}$. According to (2.19), the population of the lower lasing level R_{bb} is negligible; therefore (2.23) for $S_{\rm coh}$ can be simplified by neglecting it. When (2.23) is substituted into (2.38), and the multiplicative constants are expressed in terms of $\sigma_{\rm ASE}$, the resulting expression for the $S_{\rm coh}$ part is

$$\frac{2\pi ik}{\epsilon}\mathcal{P}_\sigma^{\rm coh}(\mathbf{x},t)=\frac{G_0}{2}\sum_\rho\frac{1}{n\delta V}\sum_{m\in\delta V(\mathbf{x})}\rho_{aa}(\mathbf{x}_m,t)e^{i(\rho-\sigma)kz_m}\times\mathcal{E}_\rho(\mathbf{x},t) \ . \tag{2.39}$$

After dropping the four-wave mixing terms ($\rho\neq\sigma$), (2.39) becomes

$$\frac{2\pi ik}{\epsilon}\mathcal{P}_\sigma^{\rm coh}(\mathbf{x},t)=\frac{G_0}{2}\mathcal{N}_a(\mathbf{x},t)\mathcal{E}_\rho(\mathbf{x},t) \ , \tag{2.40}$$

$$\mathcal{N}_a(\mathbf{x},t)=\frac{1}{n\delta V}\sum_{m\in\delta V(\mathbf{x})}\rho_{aa}(\mathbf{x}_m,t) \ , \tag{2.41}$$

where $\mathcal{N}_a$ is the fractional occupation of the excited state a, and $G_0\mathcal{N}_a$ is the saturated gain. The noise term in (2.26) yields

$$S_\sigma(\mathbf{x},t)\equiv\frac{2\pi ik}{\epsilon}\mathcal{P}_\sigma^{\rm noise}(\mathbf{x},t)=\frac{2\pi ik\mu_{ba}}{\epsilon}\frac{1}{\delta V}\sum_{m\in\delta V(\mathbf{x})}\tilde\Gamma_{ba}(\mathbf{x}_m,t)e^{-i\sigma kz_m} \ . \tag{2.42}$$

Combining (2.40) and (2.42) with (2.3) gives the macroscopic propagation equation

$$\left[\sigma\frac{\partial}{\partial z}+\frac{1}{c_0}\frac{\partial}{\partial t}-\frac{i}{2k}\nabla^2\right]\mathcal{E}_\sigma = \frac{G_0}{2}\mathcal{N}_a(\mathbf{x},t)\mathcal{E}_\sigma(\mathbf{x},t)+S_\sigma(\mathbf{x},t)\ . \quad (2.43)$$

The material response is described by applying the same coarse-graining procedure to (2.31), with the result

$$\frac{\partial}{\partial t}\mathcal{N}_a = w_P - \left[w_P+\gamma_a+\frac{\gamma_a}{I_0}\sum_\sigma I_\sigma\right]\mathcal{N}_a\ . \quad (2.44)$$

A similar argument yields the propagation equation for the classical pump wave:

$$\left[\frac{\partial}{\partial x}+\frac{1}{c_0}\frac{\partial}{\partial t}-\frac{i}{2k_P}\nabla^2\right]\mathcal{E}_P = -\frac{\kappa_{P0}}{2}\langle\mathcal{N}_g\rangle\mathcal{E}_P\ , \quad (2.45)$$

where $\kappa_{P0}=n\sigma_{\rm abs}$, $\sigma_{\rm abs}$ is the absorption cross section at the pump wavelength, and the conservation of population gives $\langle\mathcal{N}_g\rangle=1-\langle\mathcal{N}_a\rangle$.

We complete this section by deriving the statistical properties of the coarse-grained noise source. From the definition (2.42) one finds

$$\langle S_\sigma^\dagger(\mathbf{x},t)S_\sigma(\mathbf{x}',t')\rangle = \left[\frac{2\pi k|\mu_{ba}|}{\epsilon}\right]^2\left[\frac{1}{\delta V}\right]^2\sum_{m\in\delta V(\mathbf{x})}\sum_{n\in\delta V(\mathbf{x}')}e^{i\sigma k(z_m-z_n)}\langle\tilde\Gamma_{ba}^\dagger(\mathbf{x}_m,t)\tilde\Gamma_{ba}(\mathbf{x}_n,t')\rangle\ . \quad (2.46)$$

The fluctuation operators for different atoms are uncorrelated; therefore (2.34) allows (2.46) to be rewritten as

$$\langle S_\sigma^\dagger(\mathbf{x},t)S_\sigma(\mathbf{x}',t')\rangle = \frac{3\pi^2}{\epsilon}\frac{\hbar\gamma_a}{k}\left[\frac{1}{\delta V}\right]^2\sum_{m\in\delta V(\mathbf{x})\cap\delta V(\mathbf{x}')}\rho_{aa}(\mathbf{x}_m,t_<)e^{-\gamma_{ab}|t-t'|}\ , \quad (2.47)$$

where we have expressed the coefficient in terms of γ_a, the Einstein A coefficient, and the sum runs over the atoms in the overlap region.

In the usual phenomenological approach, one would assume that the sources are δ correlated in space, and the right-hand side of (2.47) would be proportional to a Dirac δ function. Our result is a coarse-grained version of this. If $\mathbf{x}$ and $\mathbf{x}'$ are sufficiently far apart, the volumes $\delta V(\mathbf{x})$ and $\delta V(\mathbf{x}')$ do not overlap, and the sum on the right-hand side of (2.47) vanishes, i.e., the noise sources at $\mathbf{x}$ and $\mathbf{x}'$ are uncorrelated. On the other hand, (2.47) differs from the standard δ-correlation model since it yields a finite result for $\mathbf{x}=\mathbf{x}'$. By treating the right-hand side of (2.47) as an integral kernel and applying it to slowly varying test functions, i.e., functions that are essentially constant across a coarse-graining volume, we show in Appendix B that this result can be restated as

$$\langle S_\sigma^\dagger(\mathbf{x},t)S_\sigma(\mathbf{x}',t')\rangle = \frac{3\pi^2}{\epsilon}\frac{\hbar\gamma_a}{k}n\langle\mathcal{N}_a(\mathbf{x},t_<)\rangle \times e^{-\gamma_{ab}|t-t'|}\delta_C^3(\mathbf{x}-\mathbf{x}')\ , \quad (2.48)$$

where we have used (2.41) to replace the sum over atoms by the coarse-graining population $\mathcal{N}_a$. The "coarse-grained δ function" $\delta_C^3(\mathbf{x}-\mathbf{x})$ is defined by its action on slowly varying test functions,

$$\int d^3x'\delta_C^3(\mathbf{x}-\mathbf{x}')f(\mathbf{x}')\approx f(\mathbf{x})\ , \quad (2.49)$$

and by its finite value for $\mathbf{x}=\mathbf{x}'$,

$$\delta_C^3(\mathbf{0})=\frac{1}{\delta V}\ . \quad (2.50)$$

The form (2.48) for the correlation function resembles the familiar phenomenological assumption of δ correlation in which $\delta_C^3(\mathbf{z})$ is replaced by the Dirac δ function; however, the finite value of $\delta_C^3(\mathbf{0})$ allows us to calculate the temporal correlation function of the noise source at a given spatial point:

$$\langle S_\sigma^\dagger(\mathbf{x},t)S_\sigma(\mathbf{x},t')\rangle = \frac{3\pi^2}{\epsilon}\frac{\hbar\gamma_a}{k}\frac{n\langle\mathcal{N}_a(\mathbf{x},t)\rangle}{\delta V}e^{-\gamma_{ab}|t-t'|}\ . \quad (2.51)$$

The strength of the noise source at a point, defined by setting $t=t'$ in (2.51), depends explicitly on the choice of the coarse-graining volume δV. This will play an important role in the next section, where we consider a finite-difference solution of the equations.

III. STOCHASTIC SIMULATION

As formulated in Sec. II, the theory of ASE is given by the (Heisenberg picture) operator field equations (2.43) and (2.44), together with the condition (2.48), defining the statistical properties of the source term. Unfortunately, these are nonlinear operator equations, which do not lend themselves to numerical methods. Alternatively, we could work with the equivalent master equation for the total density operator, and then choose a representation which would yield a generalized Fokker-Planck equation.[10] No effective numerical solution methods exist for such functional differential equations. The most common escape from this dilemma is to assume that the Fokker-Planck equation is equivalent to a set of Langevin equations for c-number stochastic fields. This assumption finds some support from the use of the positive-P representation, but there are still some apparent difficulties.[12] In the absence of a completely rigorous argument, we will simply adopt this assumption and replace the operator equations with c-number stochastic equations. the stochastic model is related to the quantum theory by impos-

ing (2.48) on the Langevin forcing term in the stochastic equations.

A. Finite-difference noise model

The noise term in (2.43) has a correlation time $1/\gamma_{ab}=T_2$; therefore, a straightforward finite-differencing scheme would require very small time steps, $\Delta t \ll T_2$. In order to avoid this difficulty, we replace the differential equation with a finite-step equation by integrating (2.43) over the integral $(t,t+\Delta t)$:

$$\mathcal{E}_\sigma(\mathbf{x},t+\Delta t)=\mathcal{E}_\sigma(\mathbf{x},t)+c_0\Delta t\left[\frac{i}{2k}\nabla^2-\sigma\frac{\partial}{\partial z}\right]\mathcal{E}_\sigma(\mathbf{x},t)$$

$$+c_0\Delta t\frac{G_0}{2}\mathcal{N}_a\mathcal{E}_\sigma(\mathbf{x},t)+\tilde{S}_\sigma(\mathbf{x},t)\ , \tag{3.1}$$

where the finite-step noise term is

$$\tilde{S}_\sigma(\mathbf{x},t)=c_0\int_t^{t+\Delta t}dt' S_\sigma(\mathbf{x},t')\ . \tag{3.2}$$

In other words, the effective noise source $\tilde{S}_\sigma(\mathbf{x},t)$ is proportional to the average of $S_\sigma(\mathbf{x},t)$ over one time step. We have also assumed that the other terms on the right-hand side of (2.43) are essentially constant in $(t,t+\Delta t)$. The statistical properties of $\tilde{S}_\sigma$ are obtained by using (2.48) to calculate the correlation function:

$$\langle \tilde{S}^*_\sigma(\mathbf{x},t)\tilde{S}_\sigma(\mathbf{x},t')\rangle=c_0^2\frac{3\pi^2}{\epsilon}\frac{n\hbar\gamma_a}{k}\times\langle\mathcal{N}_a(\mathbf{x},t_<)\rangle Q(t-t')\times\delta_C^3(\mathbf{x}-\mathbf{x}')\ , \tag{3.3}$$

$$Q(t-t')=\int_t^{t+\Delta t}dt_1\int_{t'}^{t'+\Delta t}dt_2 e^{-\gamma_{ab}|t-t'|}\ . \tag{3.4}$$

The integral (3.4) can be evaluated explicitly, and for $|t-t'|>\Delta t$ it has the simple form

$$Q(t-t')=\frac{2[\cosh(\gamma_{ab}\Delta t)-1]}{\gamma_{ab}^2}e^{-\gamma_{ab}|t-t'|}\ . \tag{3.5}$$

For a practical computation scheme, we can assume $\gamma_{ab}\Delta t\gg 1$; therefore, the correlations between sources more than one time step apart are exponentially small. On the other hand, for sources at adjacent time points, i.e., with $|t-t'|=\Delta t$, the exponentials cancel and (3.5) yields

$$Q(\Delta t)=\frac{1}{\gamma_{ab}^2}\ . \tag{3.6}$$

This last result should be compared to the strength of the source at a given space-time point; this is proportional to $Q(0)$, and

$$Q(0)=\frac{2\Delta t}{\gamma_{ab}}-\frac{2}{\gamma_{ab}^2}(1-e^{-\gamma_{ab}\Delta t})\approx\frac{2\Delta t}{\gamma_{ab}}\ . \tag{3.7}$$

By comparing (3.6) and (3.7), we see that the correlation between adjacent time points is weak compared to the strength at a point, i.e.,

$$\frac{Q(\Delta t)}{Q(0)}=\frac{1}{2\gamma_{ab}\Delta t}\ll 1\ ; \tag{3.8}$$

therefore, we may regard the sources at distinct time points as effectively uncorrelated.

We next turn to the relation between the coarse-graining volume δV and the spatial grid with dimensions $\Delta x,\Delta y,\Delta z$. An obviously necessary condition is $\Delta x\Delta y\Delta z\geq\delta V$, i.e., the volume of the unit grid cell cannot be smaller than the coarse-graining volume. On the other hand, if the grid spacings are too large the finite-difference scheme will not accurately represent the spatial variation of the envelope fields. On this basis, we conclude that the optimum choice for the numerical grid is to equate the unit cell and the coarse-graining volume:

$$\delta V=\Delta x\Delta y\Delta z\ . \tag{3.9}$$

An alternative argument leading to this conclusion follows from recognizing that the finite-difference scheme amounts to the assumption that the fields are piecewise continuous, with jumps at the grid cell boundaries. This is clearly a particular form of coarse-graining, so we are again led to (3.9) as the optimuum choice. For example, we can imagine each grid point at the center of a coarse-graining cube with edges $\Delta x,\Delta y,\Delta z$, so that the faces of the cube will lie halfway between adjacent grid points. Then the only atoms belonging to two different coarse-graining volumes are those which happen to lie on one of the faces. Since the cubes contain many atoms, these surface effects can be neglected, and the presence of the coarse-grained δ function in (3.3) implies that sources at different grid points are uncorrelated. Combining all these considerations shows that the sources at distinct space-time grid points can be treated as uncorrelated. Under these circumstances, the only relevant parameter is the strength of the source term at a given point on the space-time grid.

We evaluate (3.3), with $\mathbf{x}=\mathbf{x}'$, $t=t'$, using the optimum choice (3.9) for δV; this gives the strength of the random source term as

$$\langle \tilde{S}^*_\sigma(\mathbf{x},t)\tilde{S}_\sigma(\mathbf{x},t)\rangle=c_0^2\frac{3\pi^2}{\epsilon}\frac{n\hbar\gamma_a}{k\delta V}\langle\mathcal{N}_a(\mathbf{x},t)\rangle\left[\frac{2\Delta t}{\gamma_{ab}}\right]\ . \tag{3.10}$$

This can be rewritten in a more useful way by introducing a factor of ω in the numerator and denominator. In this way we get[8]

$$\langle \tilde{S}^*_\sigma(\mathbf{x},t)\tilde{S}_\sigma(\mathbf{x},t)\rangle=K\langle\mathcal{N}_a(\mathbf{x},t)\rangle\ , \tag{3.11}$$

$$K=\left[\frac{2\pi}{\epsilon c_0}\right]\left[3\pi n\frac{\gamma_a}{\gamma_{ab}}\hbar\omega c_0\right]\left[\frac{c_0\Delta t}{\Delta z}\right]\left[\frac{1}{K^2\Delta x\Delta y}\right]\ . \tag{3.12}$$

The first factor in K converts intensities into the squares of field strengths, and the second factor may be interpreted as the intensity due to noise photons. This follows from the observation that the number of photons emitted per atom in one dephasing time is $\gamma_a T_2=\gamma_a/\gamma_{ab}$. The third factor in K will be unity when the natural grid

choice $\Delta z = c_0 \Delta t$ is made. The fourth factor is determined by conditions required for the proper treatment of paraxial diffraction. The diffraction angles for radiation emitted through the $(\Delta x, \Delta y)$ face of δV are determined by the uncertainty principle:

$$\Delta x \, \Delta k_x = \Delta x k \Delta \theta_x \approx 1 \ , \tag{3.13}$$

$$\Delta y \, \Delta k_y = \Delta y k \Delta \theta_y \approx 1 \ . \tag{3.14}$$

On the other hand, a simple ray-tracing argument shows that the end-fire modes represented by the fields $\mathcal{E}_\sigma$ correspond to bundles of rays filling the geometrical opening angles $\beta_x = d/L$ and $\beta_y = h/L$. In order for the wave theory to recover this result, the diffraction angles must satisfy

$$\Delta \theta_x \geq \beta_x, \quad \Delta \theta_y \geq \beta_y \ , \tag{3.15}$$

which, in combination with (3.13) and (3.14), yields

$$k^2 \Delta x \, \Delta y \leq \frac{1}{\beta_x \beta_y} \ . \tag{3.16}$$

For reasons of economy, we want the coarse-graining volume to be as large as possible; therefore, we define the noise source by choosing Δx and Δy to satisfy the equality in (3.16), and thereby obtain

$$k^2 \Delta x \, \Delta y = \frac{L}{d} \frac{L}{h} = \frac{1}{\Omega} \ , \tag{3.17}$$

where $\Omega = hd/L^2$ is the solid angle subtended by the output face. This yields the final form for K:

$$K = \left[\frac{2\pi}{\epsilon c_0} \right] (3\pi n \hbar \omega \gamma_a c_0 \gamma_{ab}^{-1}) \Omega \ . \tag{3.18}$$

The factor Ω represents the dependence of the source on the amplifier geometry; thus the *ad hoc* insertion of a solid-angle factor, as done for plane-wave theories, is eliminated. Also note that the general theory of stochastic differential equations would lead us to expect an integrated noise term proportional to $(c_0 \Delta t)^{1/2}$, but our analysis yields instead

$$(c_0 \Delta t)^{1/2} \rightarrow (c_0 \gamma_{ab}^{-1})^{1/2} = (c_0 T_2)^{1/2} \ , \tag{3.19}$$

that is, the differential Δt which would appear in a phenomenological stochastic treatment is replaced by the physical parameter T_2.

B. Numerical methods

The theory is formulated generally for propagation in the time and three spatial dimensions; however, we limit our numerical calculations to the time and two spatial dimensions, namely the z axis and the x axis. We show in Appendix C that this requires a modification of the noise source in which K is replaced by

$$\overline{K} = \left[\frac{2\pi}{\epsilon c_0} \right] (3\pi n \hbar \omega \gamma_a c_0 \gamma_{ab}^{-1}) \frac{\beta_x}{kh} \ , \tag{3.20}$$

where β_x is the opening angle d/L and h is the y dimension of the sample. For the simulation, the noise source at a given space-time grid point is given by

$$\tilde{S}_\sigma(x_i, z_j, t_k) = [\overline{K} \mathcal{N}_a(x_i, z_j, t_k)]^{1/2} \xi_\sigma(i,j,k) \ , \tag{3.21}$$

where $\xi_\sigma(i,j,k)$ is a complex number chosen independently, for each wave at each lattice site, from a Gaussian distribution with unit average square modulus. The fluctuating quantity $\mathcal{N}_a$ should, strictly speaking, be replaced by its ensemble average, but we will assume that $\mathcal{N}_a - \langle \mathcal{N}_a \rangle$ is small so that we can neglect this refinement. We approximate the choice of $\xi_\sigma(i,j,k)$ by setting

$$\xi_\sigma(i,j,k) = \frac{1}{\sqrt{2}} (\alpha + i\beta) \ , \tag{3.22}$$

and drawing α and β from an approximately normal distribution with unit variance constructed by means of the central limit theorem.[13]

For the ASE equations, whose bidirectional nature means that the time and propagation direction must be treated as separate, independent variables to achieve complete generality, we use the Peaceman-Rachford (PR) alternating-direction-implicit (ADI) algorithm.[14] This method applies to partial differential equations (PDE) having parabolic form. It has received wide application recently to integrate the Schrödinger equation for an atom in the presence of a strong electromagnetic field.[15] Our ASE equations are parabolic in form, except for the first-order z derivatives. However, we modify the PR method simply by representing this derivative by a two-point forward or backward difference, as appropriate at boundaries. The second-order x derivative is represented by the usual three-point central difference. Then the z and x derivatives, suitably represented by differences, are alternated as implicit or explicit in the PR scheme. The PR method uses reflective boundary conditions which will give rise to spurious reflections from the numerical grid boundaries. To avoid this, absorbing terms localized at the grid boundaries are added to the paraxial equation. The overall solution method treats the derivative terms by a stable implicit scheme, but the nonlinear gain term, the source term, and the absorbers are treated explicitly. The method is sufficiently general that the second-order z derivatives, which would describe a reflective component in the wave, could be retained. The pump action, with propagation along x and diffraction along z, is solved in the retarded-time frame, in which it has the standard parabolic form, using the Cranck-Nicolson algorithm.

Most of the sample calculations presented below were carried out in conjunction with an experimental program using laser-pumped dye solutions. The dye sample in these experiments has the dimensions $d \approx 0.06$ cm, $h \approx 0.02$ cm, and $L \approx 2.1$ cm, so the "solid-angle factor" (β_x/kh) in (3.20) is 9×10^{-6}. The dye is pumped by an injection-seeded, frequency-doubled Nd:YAG laser (YAG denotes yttrium aluminum garnet), so the ASE propagation equations, the transverse pump propagation equations, and the material response equations must be solved self-consistently. Our experience shows that the numerical solutions given here are reliable for $\Delta x = 6 \times 10^{-4}$ cm and $\Delta z = 2.4 \times 10^{-2}$ cm. The value of

Δx used in integrating the equations is about three times larger than the optimum value used in the definition of the coarse-grained noise source by (3.20). We employ a dimensionless time $\gamma_a t$; therefore, the large factor c_0/γ_a weights all terms on the right-hand side of (3.1). This requires a small step size $\gamma_a \Delta t = 6.1 \times 10^{-4}$. If the temporal step size is not small enough, then the z profiles for the population $\mathcal{N}_a$ exhibit numerical noise; consequently, we generally take smooth z profiles of $\mathcal{N}_a$ as our primary test of numerical accuracy.

IV. APPLICATIONS

A. Saturation in strongly inverted media

The gain associated with the lasing transition $a \rightarrow b$ is proportional to the average population difference $\rho_{aa} - \rho_{bb}$, but in a strongly inverted medium $\rho_{aa} \gg \rho_{bb}$. This means that the saturated gain is given by

$$G = G_0 N_a \ , \tag{4.1}$$

where $N_a \equiv \langle \mathcal{N}_a \rangle$ is the average fractional occupation. We can estimate N_a by means of the semiclassical limit of (2.44), i.e., we take the ensemble average and assume that

$$\langle \mathcal{N}_a \mathcal{I}_\sigma \rangle \approx N_a I_a \ , \tag{4.2}$$

where $I_a \equiv \langle \mathcal{I}_a \rangle$ is the average intensity. This leads to

$$\frac{\partial}{\partial t} N_a = w_P - \left[w_P + \gamma_a + \frac{\gamma_a}{I_0} \sum_\sigma I_\sigma \right] N_a \ . \tag{4.3}$$

The stationary solution of (4.3), together with (4.1) gives the following result for the saturated gain:

$$G = G_0 N_a = G_0 \frac{w_p}{w_P + \gamma_a + \frac{\gamma_a}{I_0} \sum_\sigma I_\sigma} = \frac{\bar{G}}{1 + \frac{I}{I_{\rm sat}}} \ , \tag{4.4}$$

where the weak signal gain and the saturation intensity are given, respectively, by

$$\bar{G} = \frac{G_0 w_P}{\gamma_a + w_P} \ , \tag{4.5}$$

$$I_{\rm sat} = \left[1 + \frac{w_P}{\gamma_a} \right] I_0 , \tag{4.6}$$

and I is the total ASE intensity

$$I = \sum_\sigma I_\sigma \ . \tag{4.7}$$

The saturation intensity $I_{\rm sat}$ is the intensity for which the gain is reduced to one half of the weak signal value; this is the conventional definition. Recall that I_0 is the intensity for which the simulated emission rate equals the spontaneous emission rate; this is the value usually quoted for the saturation intensity. The modified value given by (4.6) is a consequence of the rapid depopulation of the lower lasing level.

For the case of laser pumping, the pump rate w_P is given by (2.13) and the saturation intensity can be expressed as

$$I_{\rm sat} = \left[1 + \frac{P}{P_0} \right] I_0 \ , \tag{4.8}$$

$$P_0 = \frac{\gamma_a \hbar \omega_P}{\sigma_P} \ , \tag{4.9}$$

where P_0 is the intensity at which the absorption rate of pump photons equals the spontaneous emission rate. This is the intensity which usually describes saturation of the absorption, but this definition also requires modification. Since the absorptivity is proportional to the ground-state occupation, it is sufficient to calculate N_g by using (4.4) and (4.9):

$$N_g = 1 - N_a = \frac{1 + I/I_0}{1 + P/P_0 + I/I_0} = \frac{1}{1 + P/P_{\rm sat}} \ . \tag{4.10}$$

Thus $P_{\rm sat}$ is the intensity at which the absorption is reduced to one half of the weak-pump limit; it is given by

$$P_{\rm sat} = P_0 \left[1 + \frac{1}{I_0} \right] . \tag{4.11}$$

This result for the pump saturation intensity and (4.8), for the ASE saturation intensity, are related by $I \leftrightarrow P$, $I_0 \leftrightarrow P_0$. We refer to this reciprocal behavior as cross saturation.

This phenomenon can be experimentally investigated by observing transverse fluorescence from the excited dye molecules and transmission of the pump radiation. The fluorescence intensity is proportional to the excited state occupation $N_a = G/\bar{G}$; therefore (4.4) shows that fluorescence will be suppressed at the ends of the amplifier where the ASE signal is strongest. Similarly, (4.11) shows that $P_{\rm sat}$ is larger at the ends, which means that more molecules are in the ground state and transmission of the pump is reduced. Thus we should expect that the fluorescence signal and the transmitted pump intensity will both peak at the center of the amplifier. In Figs. 2 and 3 we show time-averaged results of calculations of N_a and N_g, corresponding to fluorescence and transmission, respectively, which exhibit this property, together with the corresponding experimental results. A more complete discussion and details of the experimental verification of this phenomenon are given elsewhere.[6]

B. Transverse coherence

One of the principal virtues of a wave-optics description is that it allows one to study the degree of transverse coherence of the ASE signals. This is essential for understanding the growth of an organized signal from quantum noise, and it is also important for applications. In this section we present some preliminary results along these lines.

A convenient measure of transverse coherence is provided by the complex degree of coherence $\gamma_{12}(x,z)$, which is defined in terms of the cross-correlation function between a field, say $\mathcal{E}_+$, and its adjoint at different transverse positions.[16] We choose coordinates so that the

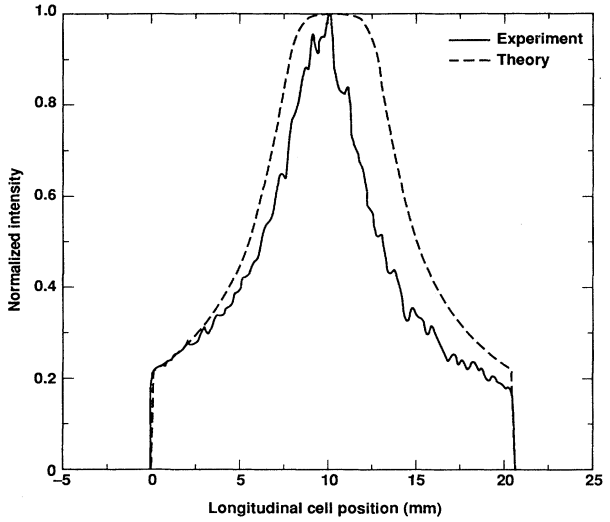

FIG. 2. Transverse fluorescence and upper lasing level population vs z. The solid curve is a simulation result for the time-integrated population of the upper lasing level, and the dotted curve shows the experimental data for the time-integrated transverse fluorescence signal (normalized to the maximum intensity).

transverse midplane of the amplifier is at $x=0$, then at the longitudinal plane z

$$\gamma_{12}(x,z)=\frac{\langle \mathcal{E}_+^*(-x/2,z)\mathcal{E}_+(x/2,z)\rangle_t}{[\langle|\mathcal{E}_+(-x/2,z)|^2\rangle_t\langle|\mathcal{E}_+(x/2,z)|^2\rangle_t]^{1/2}}\ , \tag{4.12}$$

where the time average $\langle\ \rangle_t$ is given by

$$\langle f(x,z)\rangle_t=\frac{1}{T}\int_0^T dt\, f(x,z,t) \tag{4.13}$$

for the suitably chosen averaging time T. For the examples to follow, we found that the time average stabilizes when T is several times larger than the longitudinal transit time.

In this connection, the experimentally interesting quantity is the visibility $\mathcal{V}(x,z)$, which is observed in two-slit interference experiments. It is defined by

$$\mathcal{V}(x,z)=\frac{I_{\max}-I_{\min}}{I_{\max}+I_{\min}}\ , \tag{4.14}$$

where $I_{\max}$ and $I_{\min}$ denote the maximum and minimum intensities observed in the interference pattern. The relation between the degree of coherence $\gamma_{12}(x,z)$ and the visibility $\mathcal{V}(x,z)$ is

$$\mathcal{V}(x,z)=\frac{2[\langle|\mathcal{E}_+(x/2,z)|^2\rangle_t\langle|\mathcal{E}_+(-x/2,z)|^2\rangle_t]^{1/2}}{\langle|\mathcal{E}_+(-x/2,z)|^2\rangle_t+\langle|\mathcal{E}_+(x/2,z)|^2\rangle_t}\times|\gamma_{12}(x,z)|\ . \tag{4.15}$$

In the fluorescence experiments reported above, both diffraction and pump absorption produce transverse variations in intensity and phase. In order to avoid this complication, we have carried out simulations in which pump absorption is neglected. Otherwise, the experimental parameters are as given before: $d\approx0.06$ cm, $h\approx0.02$ cm, and $L\approx2.1$ cm, $n\approx2\times10^{17}$ cm^{-3}, $G_0\approx40$ cm^{-1}.

In the next two figures we show results for both strong ($w_P/\gamma_a\gg1$) and weak ($w_P/\gamma_a\ll1$) pumping. In Fig. 4 we plot the visibility at the output face as a function of slit separation for a dimensionless pumping rate $w_P/\gamma_a=5.18$. This corresponds, by Eq. (4.5), to a weak

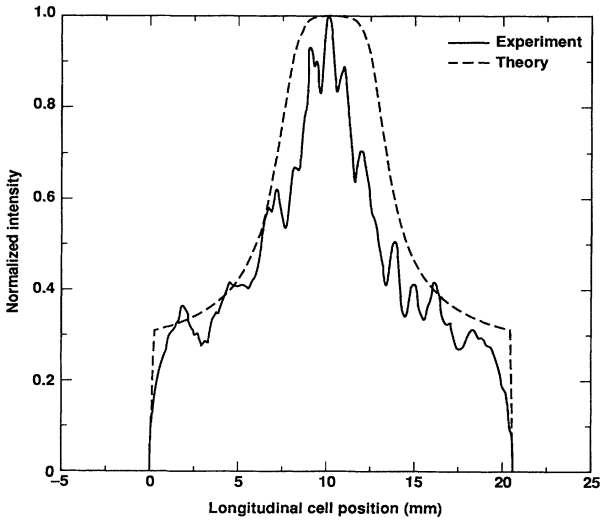

FIG. 3. Transmitted pump intensity and ground-state population vs z. The solid curve is a simulation result for the time-integrated ground-state population, and the dotted curve shows the experimental data for the time-integrated transmitted pump, normalized to the maximum intensity.

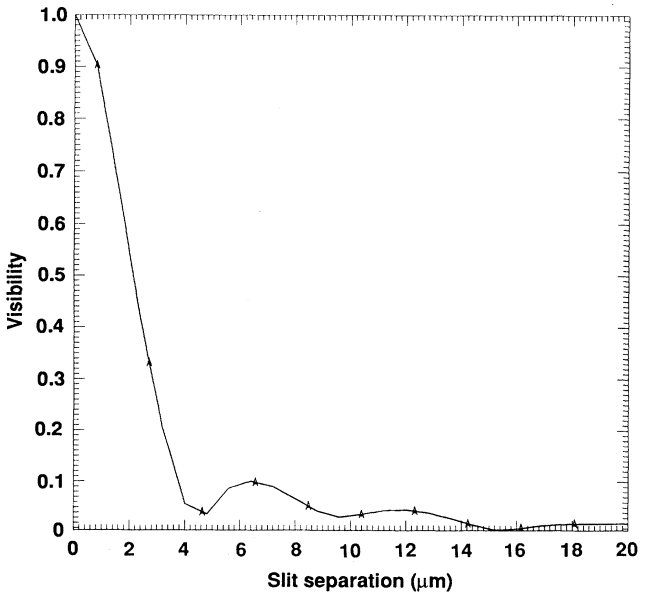

FIG. 4. Visibility vs slit separation for ASE output. This is a strong-pump ($w_P/\gamma_a=5.18$), high-gain ($\bar{G}=33.5$ cm^{-1}) case.

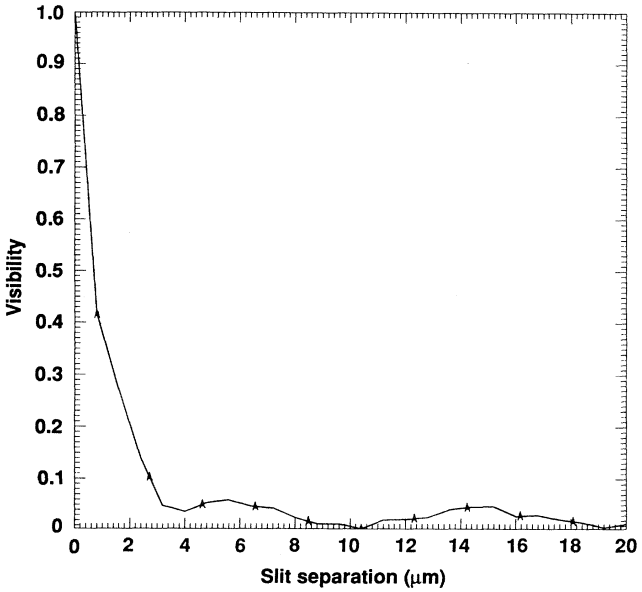

FIG. 5. Visibility vs slit separation for ASE output. This is a weak-pump ($w_P/\gamma_a=0.09$), low-gain ($\bar{G}=3.4\ \mathrm{cm}^{-1}$) case.

signal gain $\bar{G}=33.5\ \mathrm{cm}^{-1}$; therefore, the gain-length product is $\bar{G}L=74$, and the system is highly saturated. The resulting visibility curve generally resembles that obtained by placing the slits in the far field region of an incoherent source.[17] This suggests a simple model in which spontaneous emission in the first gain length (at the far end of the sample) provides the source, and the rest of the sample merely serves as the amplifying medium. This model must be viewed with some caution, since certain details of the visibility curve do not correspond to the incoherent case. In particular, the visibility at the first minimum in Fig. 4 is not zero. According to (4.14) this means that the complex degree of coherence, $\gamma_{12}(x)$, does not vanish at this point; i.e., the effective source is not completely incoherent. In Fig. 5 we show the same curve for a weak pump ($w_P/\gamma_a=0.09$), corresponding to $\bar{G}=3.4\ \mathrm{cm}^{-1}$. This gives $\bar{G}L=7.5$, so the system is unsaturated. This curve is qualitatively similar to the previous one, but we note that the central peak is much narrower, suggesting a reduced coherence length. Let Δx be the width of the central peak at half maximum; we will adopt this as a crude measure of the coherence length. For the high-gain case shown in Fig. 4, $\Delta x=21\ \mu$m, and for the low-gain case of Fig. 5, $\Delta x=7\ \mu$m. Thus the ASE output from the high-gain, saturated sample has a coherence length three times higher than that of the low-gain, unsaturated sample.

V. SUMMARY

The radiative transitions in rhodamine 6G dye lasers, which are important for ASE, involve states lying in vibration-rotation bands that form quasicontinua. We have modeled this by an effective four-level atom made up of fictitious isolated levels with phenomenologically assigned widths. From this model the strength of the dipole fluctuations is derived by using the fluctuation dissipation theorem, and the assumed rapid decay of the dipole (small T_2) is used to reduce the atomic Bloch equations to a single rate equation for the population N_a of the upper laser level. We then carry out a coarse-graining of the theory using volume δV and time T. This procedure yields the macroscopic polarization as the sum of a coherent part, driven by the two counter propagating ASE fields, and a noise term arising from the dipole fluctuations. The normalization of the noise strength is determined by the microscopic theory and depends explicitly on the coarse-graining volume.

In the formulation of the stochastic simulation scheme, we argue that the optimum choice is to set the coarse-graining volume equal to the volume of a unit grid cell. For practical computation schemes with time steps $\Delta t \gg T_2$ it then follows that the noise sources at each space-time grid point can be treated as uncorrelated. By requiring that the opening angle for radiation from a unit grid cell is at least as large as the geometrical opening angle for the sample, we show that the strength of the noise source at a grid point is proportional to the solid angle subtended by one output face. The resulting stochastic paraxial equations for the ASE fields are solved by a variant of the Peaceman-Rachford alternating-direction-implicit algorithm. This is done simultaneously with the solution of the rate equation for N_a and the paraxial equation describing pump wave propagation.

By examining the stationary solutions of the atomic rate equation we showed that the ASE saturation intensity depends on the pump intensity, and, conversely, that the saturation intensity for pump absorption depends on the ASE intensity. In this system, ASE gain and pump absorptivity are proportional to the populations N_a and $N_g=1-N_a$, respectively. This allowed the complementary relation between ASE saturation and pump saturation to be checked experimentally by measurements of transverse fluorescence and pump transmission. Our numerical simulations are in substantial agreement with the measured values.

For the simpler case of uniform pumping, we have carried out calculations of the complex degree of transverse coherence, and thereby obtained predictions for the visibility of the diffraction pattern produced by illuminating two slits with the output ASE light. The visibility curves roughly resemble those associated with diffraction using the far field of a finite incoherence source, but there are important differences in the details. The diffraction patterns obtained from the simulation do not display any true nulls in the visibility, which indicates that the effective source is not completely incoherent. Comparison of the visibility curves for an unsaturated case with small weak signal gain and a heavily saturated case with large weak signal gain show that increased gain leads to increased transverse coherence of the ASE output.

In future work we will use the simulation code to see how the transverse coherence depends on the various parameters that enter into the problem. We will also improve the theory by including the formation of interference gratings through wave mixing between the counter-propagating ASE signals.

ACKNOWLEDGMENTS

We are pleased to acknowledge very useful conversations with Mike Feit, Joe Fleck, Rodger Minich, and Ewan Wright. This work was performed under the auspices of the U.S. Department of Energy by the Lawrence Livermore National Laboratory under Contract No. W-7405-Eng-48.

APPENDIX A

In this appendix we will show that the noise terms $\Gamma_{\alpha\alpha}$ associated with the population operators are small compared to the dipole fluctuation operator Γ_{ba}. In the notation employed in QASE, we have

$$\langle \Gamma_{\alpha\alpha}(t)\Gamma_{\alpha\alpha}(t')\rangle = \Phi_\alpha \delta(t-t') , \tag{A1}$$

$$\langle \Gamma_{ba}^\dagger(t)\Gamma_{ba}(t')\rangle = \Phi_{ab}\delta(t-t') . \tag{A2}$$

For the four-level model used here, the coefficients are

$$\Phi_h = w_P \rho_{gg} + \gamma_h \rho_{hh} , \tag{A3}$$

$$\Phi_a = \gamma_h \rho_{hh} + \gamma_a \rho_{aa} , \tag{A4}$$

$$\Phi_b = \gamma_a \rho_{aa} + \gamma_b \rho_{bb} , \tag{A5}$$

$$\Phi_b = w_P \rho_{gg} + \gamma_b \rho_{bb} , \tag{A6}$$

$$\Phi_{ab} = \gamma_b \rho_{aa} + \gamma_h \rho_{hh} , \tag{A7}$$

where $\rho_{\alpha\alpha} = \langle R_{\alpha\alpha}\rangle$ is the average population. We estimate these coefficients averaging the operator equations (2.7)–(2.11) and obtaining the stationary solutions in the weak signal limit. This leads easily to

$$\rho_{\beta\beta} \approx \frac{w_P/\gamma_\beta}{1+w_P/\gamma_a}, \quad \beta = h,a,b , \tag{A8}$$

$$\rho_{gg} = \frac{1}{1+w_P/\gamma_a} . \tag{A9}$$

Substituting these estimates into (A3)–(A7) gives

$$\Phi_\alpha = \frac{2w_P}{1+w_P/\gamma_a}, \quad \alpha \in \{h,b,a,g\} , \tag{A10}$$

$$\Phi_{ab} = \frac{\gamma_b}{\gamma_a}\frac{w_P}{1+w_P/\gamma_a} . \tag{A11}$$

Therefore

$$\frac{\Phi_\alpha}{\Phi_{ab}} = 2\frac{\gamma_a}{\gamma_b} \ll 1 , \tag{A12}$$

where the inequality results from the adiabaticity condition (2.15). This shows that the Langevin terms $\Gamma_{\alpha\alpha}$ appearing in the population equations are small compared to the Langevin term Γ_{ba} for the dipole transition operator.

APPENDIX B

Here we derive Eq. (2.48), the coarse-grained δ-correlated form for Eq. (2.47). Define the integral kernel $\Delta(\mathbf{x},t;\mathbf{x}',t')$ to be the right-hand side of (2.47), which we rewrite in the equivalent form

$$\Delta(\mathbf{x},t;\mathbf{x}',t') = \frac{3\pi^2}{\epsilon}\frac{\hbar\gamma_a}{k}\left[\frac{1}{\delta V}\right]^2 \times \sum_m \rho_{aa}(\mathbf{x}_m, t_<) e^{-\gamma_{ab}|t-t'|} \times \chi_m(\mathbf{x})\chi_m(\mathbf{x}') , \tag{B1}$$

where $\chi_m(\mathbf{x})$ is defined by

$$\chi_m(\mathbf{x}) = \begin{cases} 1 & \text{for } m \in \delta V(\mathbf{x}) \\ 0 & \text{otherwise} \end{cases}$$

$$= \int_{\delta V(\mathbf{x})} d^3r \, \delta(\mathbf{r}-\mathbf{x}_m)$$

$$= \int_{\delta V(0)} d^3r \, \delta(\mathbf{r}+\mathbf{x}-\mathbf{x}_m) . \tag{B2}$$

Now, regarding (B1) as an integral kernel in $\mathbf{x}$ and $\mathbf{x}'$, we multiply by a function $f(\mathbf{x}')$ and integrate over $\mathbf{x}'$. According to (B1), this requires the calculation of

$$\int d^3\mathbf{x}' \chi_m(\mathbf{x}') f(\mathbf{x}') = \int d^3\mathbf{x}' \int_{\delta V(0)} d^3r \, \delta(\mathbf{r}+\mathbf{x}'-\mathbf{x}_m) f(\mathbf{x}') = \int_{\delta V(0)} d^3r f(\mathbf{x}_m - \mathbf{r}) \approx \delta V f(\mathbf{x}_m) , \tag{B3}$$

where the last line is valid for functions that are essentially constant across a coarse-graining volume. Combining (B3) with (B1) yields

$$\int d^3\mathbf{x}' \Delta(\mathbf{x},t;\mathbf{x}',t') f(\mathbf{x}') \approx \frac{3\pi^2}{\epsilon}\frac{\hbar\gamma_a}{k}\left[\frac{1}{\delta V}\right] \sum_{m\in\delta V(\mathbf{x})} \rho_{aa}(\mathbf{x}_m, t_<) f(\mathbf{x}_m)$$

$$\approx \frac{3\pi^2}{\epsilon}\frac{\hbar\gamma_a}{k} n \langle \mathcal{N}_a(\mathbf{x}, t_<)\rangle f(\mathbf{x}) , \tag{B4}$$

where the final line was obtained by using the slow variation of $f(\mathbf{x})$ and the definition of the coarse-grained population given by Eq. (2.41). This shows that $\Delta(\mathbf{x},t;\mathbf{x}',t')$ behaves like a δ function when applied to slowly varying test functions. If we define a coarse-grained δ function $\delta_c^3(\mathbf{x}-\mathbf{x}')$ by its action on slowly varying functions,

$$\int d^3x' \delta_C^3(\mathbf{x}-\mathbf{x}') f(\mathbf{x}') \approx f(\mathbf{x}) , \tag{B5}$$

then $\Delta(\mathbf{x},t;\mathbf{x}',t')$ is clearly proportional to $\delta_C^3(\mathbf{x}-\mathbf{x}')$, at least for $\mathbf{x}\neq\mathbf{x}'$. The finite value of $\Delta(\mathbf{x},t;\mathbf{x}',t')$ at $\mathbf{x}=\mathbf{x}'$ can be included by defining

$$\delta_C^3(\mathbf{0}) = \frac{1}{\delta V} , \tag{B6}$$

then combining (B6), (B5), and (B4) gives Eq. (2.48).

APPENDIX C

Here we will show how to modify the source term, derived in Sec. III A for the three-dimensional theory, to deal with the restricted calculation in which one spatial dimension is neglected. We begin with the finite time step equation (3.1) and average it over y using the definition

$$\langle f(\mathbf{x},t)\rangle_y \equiv \frac{1}{h}\int_0^h dy f(\mathbf{x},t) . \tag{C1}$$

This gives

$$\mathcal{E}_\sigma(x,z,t+\Delta t) = \mathcal{E}_\sigma(x,z,t) + c_0\Delta t\left[\frac{i}{2k}\frac{\partial^2}{\partial x^2} - \sigma\frac{\partial}{\partial z}\right]\mathcal{E}_\sigma(x,z,t)$$

$$+ c_0\Delta t\frac{G_0}{2}\langle \mathcal{N}_a(\mathbf{x},t)\mathcal{E}_\sigma(\mathbf{x},t)\rangle_y + \tilde{S}_\sigma(x,z,t) + c_0\Delta t\frac{i}{2kh}\frac{\partial \mathcal{E}_\sigma(\mathbf{x},t)}{\partial y}\Bigg|_0^h , \tag{C2}$$

where the new fields and sources are given by

$$\mathcal{E}_\sigma(x,z,t) \equiv \langle \mathcal{E}_\sigma(\mathbf{x},t)\rangle_y , \tag{C3}$$

$$\tilde{S}_\sigma(x,z,t) \equiv \langle \tilde{S}_\sigma(\mathbf{x},t)\rangle_y . \tag{C4}$$

The necessary approximations are to drop the final term in (C2) and to assume

$$\langle \mathcal{N}_a(\mathbf{x},t)\mathcal{E}_\sigma(\mathbf{x},t)\rangle_y \approx \langle \mathcal{N}_a(\mathbf{x},t)\rangle_y \langle \mathcal{E}_\sigma(\mathbf{x},t)\rangle_y . \tag{C5}$$

Thus (C2) is replaced by

$$\mathcal{E}_\sigma(x,z,t+\Delta t) = \mathcal{E}_\sigma(x,z,t) + c_0\Delta t\left[\frac{i}{2k}\frac{\partial^2}{\partial x^2} - \sigma\frac{\partial}{\partial z}\right]\mathcal{E}_\sigma(x,z,t) + c_0\Delta t\frac{G_0}{2}\mathcal{N}_a(x,z,t)\mathcal{E}_\sigma(x,z,t) + \tilde{S}_\sigma(x,z,t) , \tag{C6}$$

and we need only calculate the strength of the new source term $\tilde{S}_\sigma(x,z,t)$. We proceed as usual from the definition (C4):

$$\langle \tilde{S}^\dagger_\sigma(x,z,t)\tilde{S}_\sigma(x,z,t)\rangle = \frac{1}{h}\int_0^h dy_1 \frac{1}{h}\int_0^h dy_2 \langle \tilde{S}^\dagger_\sigma(x,y_1,z,t)\tilde{S}_\sigma(x,y_2,z,t)\rangle . \tag{C7}$$

We also need (3.3) evaluated at $t=t'$:

$$\langle \tilde{S}^*_\sigma(\mathbf{x},t)\tilde{S}_\sigma(\mathbf{x}',t)\rangle = c_0^2\frac{3\pi^2}{\epsilon}\frac{n\hbar\gamma_a}{k}\langle \mathcal{N}_a(\mathbf{x},t)\rangle\frac{2\Delta t}{\gamma_{ab}}\delta_C^3(\mathbf{x}-\mathbf{x}') , \tag{C8}$$

and

$$\delta_C^3(\mathbf{x}-\mathbf{x}') = \delta_C(x-x')\delta_C(y-y')\delta_C(z-z') . \tag{C9}$$

From the last equation we see that

$$\delta_C^3(\mathbf{x}-\mathbf{x}') \to \frac{\delta_C(y-y')}{\Delta x\,\Delta z} \quad \text{as } x\to x',\ z\to z' ; \tag{C10}$$

therefore, inserting (C8) and (C10) into (C7) gives

$$\langle \tilde{S}^\dagger_\sigma(x,z,t)\tilde{S}_\sigma(x,z,t)\rangle = c_0^2\frac{3\pi^2}{\epsilon}\frac{n\hbar\gamma_a}{k}\langle \mathcal{N}_a(x,z,t)\rangle\frac{2\Delta t}{\gamma_{ab}}\frac{1}{h\,\Delta x\,\Delta z} , \tag{C11}$$

which differs from the three-dimensional result (3.10) only by the replacement $\Delta y \to h$. This means that the result (3.12) for K is changed by the replacement $k^2 \Delta x \Delta y \to k^2 \Delta x h$, and the diffraction argument now becomes

$$k\Delta x = \frac{L}{d} = \frac{1}{\beta_x} \ . \tag{C12}$$

Combining these results finally gives the new value for K:

$$\bar{K} = \left[\frac{2\pi}{\epsilon c_0} \right] (3\pi n \hbar \omega \gamma_a c_0 \gamma_{ab}^{-1}) \frac{\beta_x}{kh} \ . \tag{C13}$$

[1]John C. Garrison, Howard Nathel, and Raymond Y. Chiao, J. Opt. Soc. Am. B **5**, 1528 (1988).

[2]F. A. Hopf and P. Meystre, Phys. Rev. A **12**, 2534 (1975).

[3]F. A. Hopf, P. Meystre, and D. W. McClaughlin, Phys. Rev. A **13**, 777 (1976).

[4]L. Allen and G. I. Peters, Phys. Rev. A **8**, 2031 (1973).

[5]U. Ganiel, A. Hardy, G. Neumann, and D. Treves, IEEE J. Quantum Electron. **QE-11**, 881 (1975).

[6]H. Nathel, C. K. Hong, J. C. Garrison, and A. B. Ritchie (unpublished).

[7]Y. T. Lee, W. M. Howard, and J. K. Nash, J. Quant. Spectrosc. Radiat. Transfer **43**, 355 (1990). References to other schemes are also given here.

[8]M. D. Feit and J. A. Fleck, J. Opt. Soc. Am. B **7**, 2048 (1990). The dependence of the noise strength on the numerical grid size is obtained in this paper by a closely related argument. We thank the authors for a copy of their work prior to publication.

[9]A. E. Siegman, *Lasers* (University Science, Mill Valley, CA, 1986).

[10]H. Haken, *Laser Theory* (Springer-Verleg, New York, 1970), Chap. IV.

[11]A. Schenzle and H. Brand, Phys. Rev. A **20**, 1628 (1979).

[12]A. M. Smith and C. W. Gardiner, Phys. Rev. A **7**, 3511 (1989).

[13]H. Risken, *The Fokker-Planck Equation*, 2nd ed. (Springer-Verlag, New York, 1989), p. 61.

[14]J. H. Ferziger, *Numerical Methods for Engineering Applications* (Wiley, New York, 1981), pp. 160 and 161.

[15]K. Kulander, Phys. Rev. A **36**, 2726 (1987); B. Ritchie, C. Bowden, C. Sung, and Y. Li, *ibid.* **41**, 6114 (1990).

[16]M. Born and E. Wolf, *Principles of Optics*, 6th ed. (Pergamon, New York, 1985), pp. 500–505.

[17]Reference 16, p. 516.